PHYSICAL REVIEW A VOLUME 50, NUMBER 2 AUGUST 1994

Self-induced planar and cylindrical splitting of a laser beam in sodium vapor

A. Gahl, J. Seipenbusch, A. Aumann, M. Möller, and W. Lange
Institut für Angewandte Physik, Westfälische Wilhelms-Universität, Corrensstrasse 2/4, 48149 Münster, Germany
(Received 11 May 1994)

An almost linearly polarized laser beam focused into a sodium vapor cell may split into different patterns ranging from two spots to a spot and a ring of opposite circular polarization. The patterns are controlled by static magnetic fields of the order of the earth's field. The behavior is explained, allowing for a longitudinal component of the dielectric polarization in the paraxial wave equation. Numerical results reveal the delicate balance between light shift, influence of the magnetic field, and the creation of ground-state orientation by the competing polarization components.

PACS number(s): 42.50.Ne, 42.50.Gy, 42.65.An

The pioneering work of Tam and Happer [1] on the self-induced planar separation of orthogonal circular polarization components in the transmission of an initially linearly polarized light beam through a sodium cell has recently been complemented by observations of the separation of an elliptically polarized beam into multiple polarized cylindrical structures [2,3]. These phenomena have been observed on resonance [3–5] and in the near-resonant dispersive regime [6–8] and how a breaking of the cylindrical symmetry can originate from spatial imperfections of the input beam has been discussed [7].

There is no doubt that the basic nonlinear mechanism responsible for the vector wave breaking in sodium vapor is the creation of an orientation in the sodium ground state by the competing polarization components. It is surprising, however, that pronounced spatial effects should be due to a mechanism which is not only easily saturated, but which is very sensitive to diffusion, since the orientation is extremely long-lived. In this paper we establish that in a subtle way the phenomenon of the light shift can provide a nonlinear mechanism that cannot be saturated and that is not sensitive to diffusion because it depends strictly locally on the intensity of the light field. We demonstrate the transition from the cylindrical to a planar symmetry of spots of different polarization which is controlled by a very weak magnetic field in a completely deterministic way. Moreover, we provide a formalism which may be found suitable to describe the propagation of a light beam in the presence of a magnetic field, and present a numerical simulation of the experiment.

The sodium vapor cell consists of a heated quartz tube with a length of 3 cm containing a small quantity of solid sodium in a nitrogen atmosphere of about $p_{N_2}=100$ mbar. Three pairs of Helmholtz coils create a static magnetic field of arbitrary strength and direction. The laser light is provided by a cw ring dye laser that is operated at a detuning of about 10 GHz above the D_1 resonance. The laser beam is spatially filtered to have a residual astigmatism of less than 1%. A maximum power P_{in} of about 200 mW can be focused into the cell. By means of a calcite polarizer and a quarter-wave plate the polarization ellipticity $\epsilon=(P_+-P_-)/(P_++P_-)$ can be adjusted to a precision of at least 0.5%. A lens on a translation stage is used to vary the focus position, i.e., the real part of the complex beam parameter at the beginning of the interaction zone, $z(w_0)$. A second lens images the intensity pattern at the end of the interaction zone onto a charge-coupled-device (CCD) camera chip. An optional polarizing unit may be inserted to image only one selected circular polarization (see Fig. 1).

Whenever there is a small deviation from linear polarization ($\epsilon\neq 0$) in the incident light beam, spatial separation of different circular polarization components with cylindrical symmetry can be observed (cf. [3]). When a weak transverse magnetic field—which may be even below the order of the earth's magnetic field—is applied, this symmetry may be broken and the cylindrical pattern continuously deformed, eventually ending up in two distinct separate spots, provided the nonlinearity is strong enough (cf. Fig. 2 for the shape of the patterns). Both polarization components propagate at opposite angles with respect to the optical axis; the shape of the pattern at different distances from the cell is qualitatively unchanged, as can be observed removing the imaging lens. If the magnetic-field strength is varied, the amount of separation will show a narrow maximum at a rather small field and decay towards large fields. The angle between the direction of this separation and the direction of the magnetic field depends on its magnitude and on the incident power in a rather complicated way. The behavior is invariant with respect to the absolute field direction within the transverse plane; any influence by initial spatial distortions in the incident beam can thus be excluded.

Applying an additional longitudinal magnetic field yields a mutual change of intensities of the two polarization components and a modification of the angle of the separation as long as the field strength is of comparable magnitude to the transverse field. With a dominating longitudinal field, however, there are only relatively small deviations from cylindrical symmetry. The dependence on the longitudinal field does

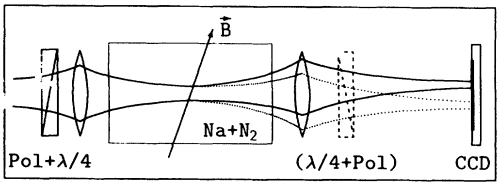

FIG. 1. Schematic experimental setup.

1050-2947/94/50(2)/917(4)/$06.00

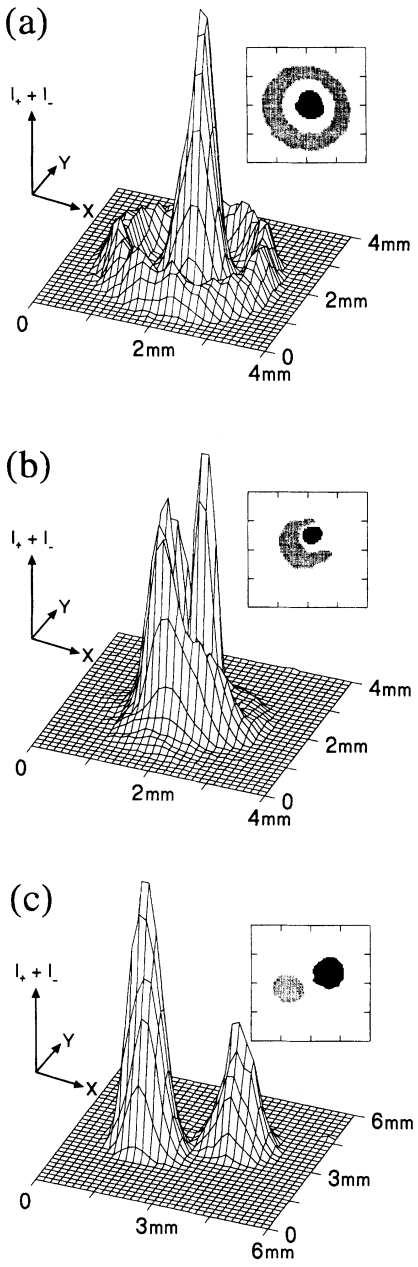

FIG. 2. Measured intensity patterns on a CCD camera. Black, I_-; gray, I_+. Experimental parameters: $\epsilon=0.05$, $N=1.2\times10^{14}$ cm^{-3}, $w_0=50$ μm (a) $B_x=-23$ μT, $B_y=80$ μT, $B_z=400$ μT, $z(w_0)=-3$ cm, $P_{in}=190$ mW, $\Delta/2\pi=15$ GHz, (b) same as (a), except $\Delta/2\pi=13$ GHz, (c) $B_x=-58$ μT, $B_y=-9$ μT, $B_z=33$ μT, $z(w_0)=0$ cm, $P_{in}=75$ mW, $\Delta/2\pi=12$ GHz,

not show a symmetry with respect to zero, the sensitivity on the transverse field is most pronounced at a certain nonzero value of the longitudinal field.

Typical patterns observed in the experiment by varying the experimental parameters are shown in Fig. 2. With a focal position corresponding to the end of the vapor cell and a rather large longitudinal magnetic field the beam splits into a central spot of the weaker incident circular polarization surrounded by a ring of the other polarization [Fig. 2(a)] [6].

When the strength of the nonlinearity is increased, e.g., by decreasing detuning or increasing particle density, the ring will become asymmetric [Fig. 2(b)]. With the position of the focus at the beginning of the cell, the beam will split into two distinct spots [Fig. 2(c)] if the transverse magnetic field is at least comparable to the longitudinal field. It turns out that the behavior is most sensitive to the position of the focus, i.e., on the fraction of the cell length with high field amplitudes yielding strongly nonlinear interaction.

The use of nitrogen as a buffer gas is necessary to suppress the influence of radiation trapping, which is known to destroy orientation in the ground state [9,10]. Most of the observations reported here are absent in an argon atmosphere, and we conclude that radiation trapping can play an important role also in beam propagation.

Since it is well known that the wave equation has to be modified in the presence of a magnetic field, we start from Maxwell's equations and obtain immediately

$$\left[\Delta-\frac{1}{c^2}\,\partial_t^2\right]\epsilon_0\mathbf{E}+\nabla(\nabla\cdot\mathbf{P})-\frac{1}{c^2}\,\partial_t^2\mathbf{P}=\mathbf{0}, \tag{1}$$

without any assumptions on the field dependence of the dielectric polarization $\mathbf{P}$. Now we assume that the electric field and the polarization can be written as

$$\mathbf{E}=\mathscr{E}\exp[-i(kz-\omega t)], \tag{2a}$$

$$\mathbf{P}=\mathscr{P}\exp[-i(kz-\omega t)] \tag{2b}$$

($k=\omega/c$ denoting the vacuum wave vector). We neglect the second derivatives of $\mathscr{E}$ and $\mathscr{P}$ with respect to $k^2\mathscr{E}$ and $k^2\mathscr{P}$; furthermore we neglect $\partial_z\mathscr{E}$ and $\partial_z\mathscr{P}$ compared to $k\mathscr{E}$ and $k\mathscr{P}$, respectively. Writing the transverse electric field as

$$\mathscr{E}_\perp=\hat{\mathbf{e}}_z\times(\mathscr{E}\times\hat{\mathbf{e}}_z), \tag{3}$$

the paraxial wave equation reads

$$2ik\partial_z\epsilon_0\mathscr{E}_\perp=\Delta_\perp\epsilon_0\mathscr{E}_\perp-ik\nabla_\perp(\hat{\mathbf{e}}_z\cdot\mathscr{P})+k^2\mathscr{P}_\perp, \tag{4}$$

with the transverse gradient of the longitudinal polarization component as an additional quantity to affect the propagation.

For the specific case here, we substitute the results for the polarization of the sodium vapor as given in [11,4]

$$\mathscr{P}=\chi_{\rm lin}\epsilon_0[\mathscr{E}+i\mathbf{m}\times\mathscr{E}], \tag{5}$$

with $\mathbf{m}$ denoting the magnetization vector and $\chi_{\rm lin}$ denoting the linear susceptibility. The latter can be computed from the sodium particle density N, the relaxation rate of the optical coherences Γ_2, and the normalized detuning $\bar{\Delta}=(\omega-\omega_{D_1})/\Gamma_2$ as in [11]

$$\chi_{\rm lin}=-\frac{N|\mu_e|^2}{2\hbar\epsilon_0\Gamma_2}\,\frac{\bar{\Delta}+i}{\bar{\Delta}^2+1}\,. \tag{6}$$

Assuming the longitudinal component of $\mathscr{E}$ to be small, we use $\mathscr{E}\approx\mathscr{E}_\perp$ as given by Eq. (3), yielding

$$\mathscr{P} \approx \chi_{\text{lin}} \epsilon_0 \{\hat{\mathbf{e}}_z \times [(\mathscr{E} \times \hat{\mathbf{e}}_z) + i(\hat{\mathbf{e}}_z \cdot \mathbf{m})\mathscr{E}] + i\hat{\mathbf{e}}_z [\mathbf{m} \cdot (\mathscr{E} \times \hat{\mathbf{e}}_z)]\}. \tag{7}$$

Due to the effects of saturation and particle diffusion the derivatives of the magnetization should be small compared to those of the light fields; thus Eq. (4) can be written as

$$2ik\partial_z \mathscr{E}_\perp = [\Delta_\perp + k^2 \chi_{\text{lin}}]\mathscr{E}_\perp - k\chi_{\text{lin}}[\mathbf{m} \cdot (\nabla_\perp - ik\hat{\mathbf{e}}_z)](\hat{\mathbf{e}}_z \times \mathscr{E}). \tag{8}$$

Transformed to circularly polarized components ($\sigma_\pm$)

$$\mathscr{E}_\pm = \frac{1}{\sqrt{2}}(\mp \mathscr{E}_x - i\mathscr{E}_y), \tag{9}$$

the equations become uncoupled:

$$\partial_z \mathscr{E}_\pm = \frac{1}{2ik}\{\Delta_\perp + k^2 \chi_{\text{lin}} \mp ik\chi_{\text{lin}}[\mathbf{m} \cdot (\nabla_\perp - ik\hat{\mathbf{e}}_z)]\}\mathscr{E}_\pm. \tag{10}$$

The stationary state of $\mathbf{m}=(u,v,w)$ under the influence of an arbitrary static magnetic field and of $\sigma_\pm$-light fields propagating in the z direction can be computed from the equations of motion (cf. [12]) as

$$u = \frac{P_+ - P_-}{\gamma_{\text{eff}}} \frac{\Omega_x \Omega_{z,\text{eff}} + \gamma_{\text{eff}} \Omega_y}{\gamma_{\text{eff}}^2 + \Omega_x^2 + \Omega_y^2 + \Omega_{z,\text{eff}}^2}, \tag{11a}$$

$$v = \frac{P_+ - P_-}{\gamma_{\text{eff}}} \frac{\Omega_y \Omega_{z,\text{eff}} - \gamma_{\text{eff}} \Omega_x}{\gamma_{\text{eff}}^2 + \Omega_x^2 + \Omega_y^2 + \Omega_{z,\text{eff}}^2}, \tag{11b}$$

$$w = \frac{P_+ - P_-}{\gamma_{\text{eff}}} \frac{\Omega_{z,\text{eff}}^2 + \gamma_{\text{eff}}^2}{\gamma_{\text{eff}}^2 + \Omega_x^2 + \Omega_y^2 + \Omega_{z,\text{eff}}^2}, \tag{11c}$$

with $P_\pm$ denoting the rates of optical pumping by $\sigma_\pm$ light, respectively. $\gamma_{\text{eff}} = \gamma + P_+ + P_-$ is an effective relaxation rate. The Ω_i denote the Larmor frequencies that correspond to the components of the static magnetic field; $\Omega_{z,\text{eff}} = \Omega_z - \bar{\Delta}(P_+ - P_-)$ includes the additional influence of the light shift. Thus the direction of $\mathbf{m}$ obviously depends both on the direction of the external magnetic field and on the local intensities $|\mathscr{E}_\pm|^2$.

Inserting these results into Eq. (10) we arrive at the paraxial wave equation

$$\partial_z \mathscr{E}_\pm = \frac{1}{2ik}\{\Delta_\perp + \chi_{\text{lin}}[k^2(1 \mp w) \mp ik(u\partial_x + v\partial_y)]\}\mathscr{E}_\pm. \tag{12}$$

The last term, which represents the influence of the longitudinal polarization component, is responsible for a change of the propagation direction that is now given by the vector $(\pm\chi_{\text{lin}}u, \pm\chi_{\text{lin}}v, 2)$ for $\sigma_\pm$ light, respectively.

The propagation of the light fields in the sample is computed by numerical integration of Eq. (12), using a split-step fast-Fourier-transform beam-propagation method (BPM) [13]. The behavior that is observed experimentally can be reproduced very well by numerical simulations (cf. Figs. 3). Regarding the parameter dependence, almost quantitative agreement can be achieved.

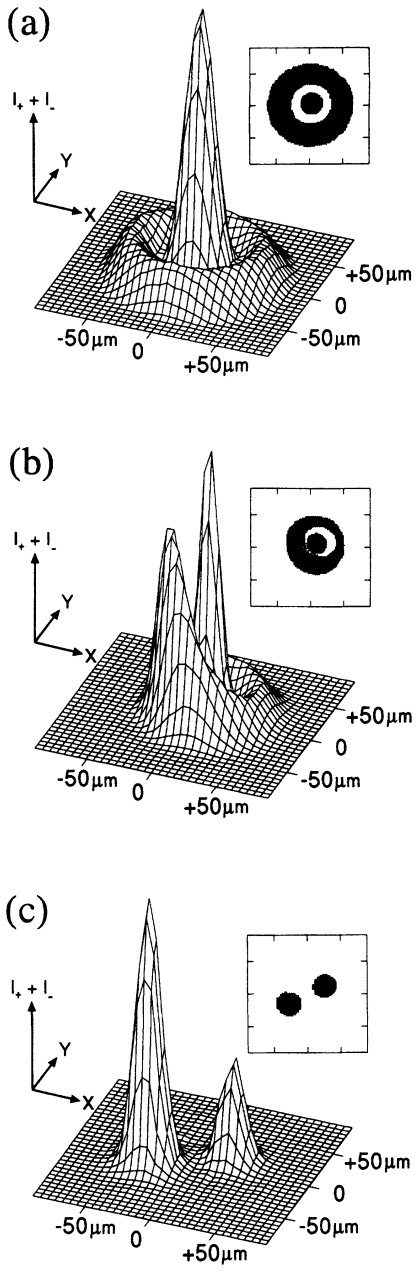

FIG. 3. Results of numerical simulation. In contrast to Fig. 2 the intensity patterns at the end of the propagation distance through the nonlinear medium are shown. Black, I_-; gray, I_+. Parameters: $\epsilon = 0.05$, $N = 1.2 \times 10^{14}$ cm^{-3}, $w_0 = 50$ μm (a) $\Omega_x/2\pi = -132$ kHz, $\Omega_y/2\pi = 459$ kHz, $\Omega_z/2\pi = 2865$ kHz, $z(w_0) = -3$ cm, $P_{in} = 190$ mW, $\Delta/2\pi = 15$ GHz; (b) same as (a), except $\Delta/2\pi = 13$ GHz; (c) $\Omega_x/2\pi = -410$ kHz, $\Omega_y/2\pi = -60$ kHz, $\Omega_z/2\pi = 230$ kHz, $z(w_0) = 0$ cm, $P_{in} = 75$ mW, $\Delta/2\pi = 12$ GHz.

The evolution of the patterns during propagation within the medium, which is not easily accessible in our experiment, turns out to be rather complicated; e.g., a pattern that eventually appears as two spots starts from a symmetric ring structure that is continuously deformed, including a rotation of the whole pattern—showing qualitatively the same sequence of patterns as in the figures. Once a conceivable de-

viation from cylindrical symmetry has developed, it is drastically amplified by the effect of mutual beam deflection already described in [8].

The interaction with the magnetic field is strongly influenced by the light shift, provided its contribution to the effective magnetic field is comparable to the external fields. The resulting variation of the local effective magnetic-field vector on short length scales strongly enhances the effect of symmetry breaking. The computed evolution of the pattern gives evidence for such a pronounced variation of these local fields in the course of propagation, mainly due to a decrease of the light-shift contribution as an increasing amount of intensity is absorbed.

Though the theoretical approach presented here still contains some coarse approximations, there is striking agreement between experiment and simulation. The diffusion of the sodium particles, which should provide the dominant decay mechanism for **m**, was formally replaced by a relaxation term γ. However, this should not lead to severe errors since we found the results to be insensitive to the value of γ. Hyperfine splitting of the D_1 transition is only allowed for by using a Landé factor of $\frac{1}{2}$ for the computation of the Larmor frequencies and by some corrections to the optical pump efficiency [12].

In summary, we have shown that the different types of self-induced separation of polarization components can be well understood by one common model. The main features of this model are the inclusion of the influence of the longitudinal polarization component on wave propagation in dielectric media and the interaction of external magnetic fields with the internal "effective" field caused by the light shift. Though the relatively simple model presented here already shows an unexpectedly good agreement with the experimental observations, further investigations are under way to take into account the influence of particle diffusion.

[1] A. C. Tam and W. Happer, Phys. Rev. Lett. **38**, 278 (1977).
[2] A. C. Wilson *et al.*, Opt. Commun. **88**, 67 (1992).
[3] D. E. McClelland *et al.*, J. Opt. Soc. Am. B **10**, 60 (1993).
[4] D. Suter, Opt. Commun. **86**, 381 (1991).
[5] D. E. McClelland, H.-A. Bachor, and J. C. Wang, Opt. Commun. **84**, 184 (1991).
[6] A. W. McCord and R. J. Ballagh, J. Opt. Soc. Am. B **7**, 73 (1990).
[7] A. W. McCord, J. Opt. Soc. Am. B **8**, 2013 (1991).
[8] R. Holzner, P. Eschle, A. W. McCord, and D. M. Warrington, Phys. Rev. Lett. **69**, 2192 (1992).
[9] G. Ankerhold *et al.*, Phys. Rev. A **48**, 4031 (1993).
[10] M. Schiffer, G. Ankerhold, E. Cruse, and W. Lange, Phys. Rev. A **49**, 1558 (1994).
[11] F. Mitschke, R. Deserno, W. Lange, and J. Mlynek, Phys. Rev. A **33**, 3219 (1986).
[12] M. Möller and W. Lange, Phys. Rev. A **49**, 4161 (1994).
[13] L. Thylén, Opt. Quantum Electron. **15**, 433 (1983).

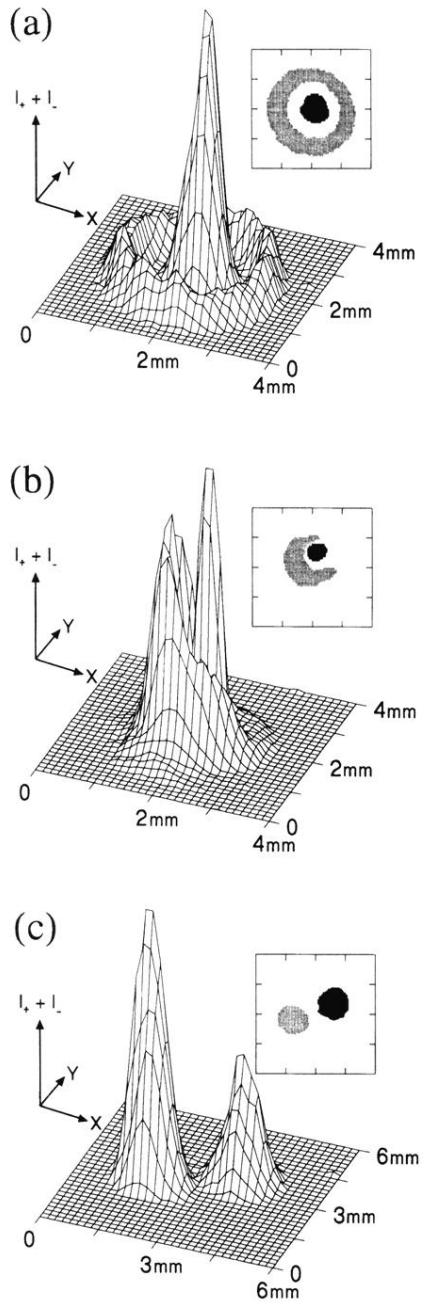

FIG. 2. Measured intensity patterns on a CCD camera. Black, I_-; gray, I_+. Experimental parameters: $\epsilon=0.05$, $N=1.2\times10^{14}$ cm^{-3}, $w_0=50$ μm (a) $B_x=-23$ μT, $B_y=80$ μT, $B_z=400$ μT, $z(w_0)=-3$ cm, $P_{in}=190$ mW, $\Delta/2\pi=15$ GHz, (b) same as (a), except $\Delta/2\pi=13$ GHz, (c) $B_x=-58$ μT, $B_y=-9$ μT, $B_z=33$ μT, $z(w_0)=0$ cm, $P_{in}=75$ mW, $\Delta/2\pi=12$ GHz,

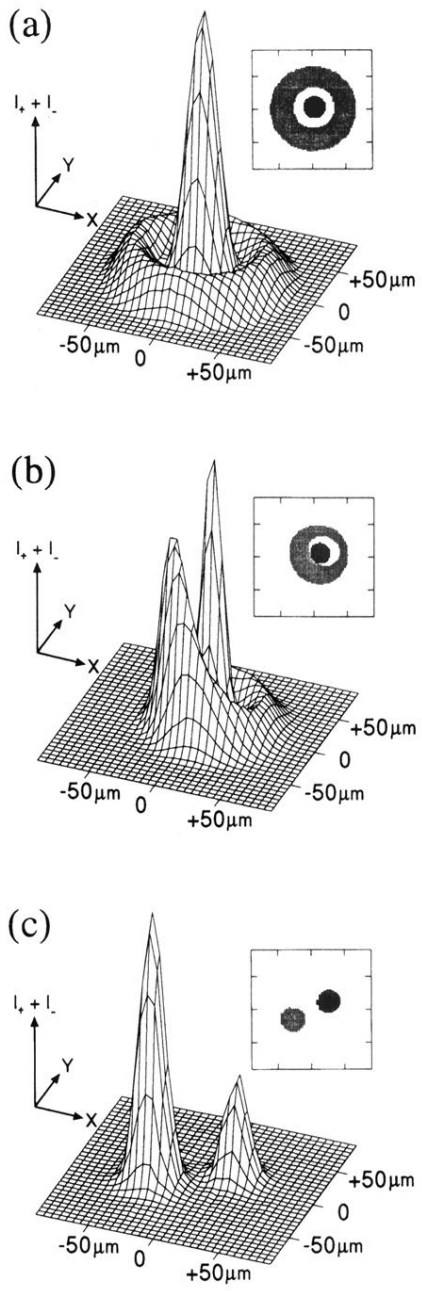

FIG. 3. Results of numerical simulation. In contrast to Fig. 2 the intensity patterns at the end of the propagation distance through the nonlinear medium are shown. Black, I_-; gray, I_+. Parameters: $\epsilon=0.05$, $N=1.2\times10^{14}$ cm^{-3}, $w_0=50$ μm (a) $\Omega_x/2\pi=-132$ kHz, $\Omega_y/2\pi=459$ kHz, $\Omega_z/2\pi=2865$ kHz, $z(w_0)=-3$ cm, $P_{in}=190$ mW, $\Delta/2\pi=15$ GHz; (b) same as (a), except $\Delta/2\pi=13$ GHz; (c) $\Omega_x/2\pi=-410$ kHz, $\Omega_y/2\pi=-60$ kHz, $\Omega_z/2\pi=230$ kHz, $z(w_0)=0$ cm, $P_{in}=75$ mW, $\Delta/2\pi=12$ GHz.